Uncharacteristic phase separation trends with the ionic size in cobaltites

J. Yu,[1] Despina Louca,[1,*] D. Phelan,[2] K. Tomiyasu,[3] K. Horigane,[3] and K. Yamada[3]
[1]*Department of Physics, University of Virginia, Charlottesville, Virginia 22904, USA*
[2]*NIST Center for Neutron Research, Gaithersburg, Maryland 20899, USA*
[3]*WPI Advanced Institute for Materials Research, Tohoku University, Katahira 2-1-1, Aoba, Sendai 980-8577, Japan*
(Received 19 July 2009; published 17 August 2009)

Using elastic neutron scattering on single crystals of $La_{1-x}A_xCoO_3$ (A=Ca^{2+}, Sr^{2+}, and Ba^{2+}), we found the development of magnetic superstructures below the global magnetic transition to be strongly dependent on the size of the A-site dopant, $\langle r_A \rangle$, in an unusual way. Upon reducing the $\langle r_A \rangle$ (i.e., as with Ca doping), only a commensurate ferromagnetic cluster phase is evident. On expanding the $\langle r_A \rangle$, the tendency toward coexistence of competing ferromagnetic and antiferromagnetic orders increases giving rise to an inhomogeneous ground state. The antiferromagnetic ordered state, initially incommensurate, continuously strengthens and becomes commensurate with long-range order and a characteristic cubic wave vector of $\vec{Q}_c$=(0.25,0.25,0.25) with x. The two competing order parameters become comparable in magnitude indicative of the phase-separated nature of the cobalt perovskite system.

DOI: 10.1103/PhysRevB.80.052402 PACS number(s): 71.30.+h, 61.05.fg, 71.70.−d

The coexistence of phases characterized by spin, charge, or orbital superstructures superimposed on a presumed homogeneous lattice[1–3] is ubiquitous in complex transition metal (TM) oxides. Emerging from subtle changes in the system, their presence has a dramatic effect on the properties[4] as observed in magnetoresistive, superconductive, and multiferroic compounds. The unusual states of matter, arising when charges are doped in a Mott insulator or from local valence fluctuations, are endemic to TM oxides. In cuprates, for instance, the suppression of the superconducting transition temperature, T_C, at the $\frac{1}{8}$th concentration with Ba doping has been linked to the appearance of spin- and charge-density waves[5] that are pinned to form stripes by adding dilute amounts of impurities such as nonmagnetic Zn.[6] In magnetite, charge ordering of Fe^{2+} and Fe^{3+} ions coupled with strong Coulomb repulsions drives the Verwey transition.[7,8] In manganites, charge-ordered and orbitally ordered states readily form when $LaMnO_3$ is doped particularly with smaller ions relative to La^{3+} (Ref. 9) such as Ca,[10,11] Pr, or Nd.[12] The organization of ordered charge arrays can explain the insulating behavior at high-doping levels[13,14] where metallic conductivity should have otherwise been present. Thus the precarious balance reached between the competing phases leads to ground states with intricate characteristics intimately related to unusual macroscopic behaviors. This is exemplified by the perovskite $La_{1-x}A_xCoO_3$, that exhibits weak magnetoresistance and the coupling of the lattice to magnetism is not at all obvious. By varying the radius at the A site, $\langle r_A \rangle$, that effectively changes the one-electron bandwidth, W (Refs. 15 and 16) or hopping integral, the tendency toward magnetic phase coexistence is investigated revealing an unusual trend.

The parent compound, $LaCoO_3$, has a nonmagnetic insulating ground state[17] in the $t_{2g}^6 e_g^0$ electronic configuration, and upon warming, ferromagnetic (FM) as well as antiferromagnetic (AFM) dynamic correlations[18] develop, indicative of the system's susceptibility to complex magnetic interactions. The introduction of holes in the lattice (with $R\bar{3}c$ symmetry) through doping leads to metallic conductivity at the percolation limit that is coupled to a magnetic transition via the double exchange (DE) mechanism.[19] However, the magnetic structure is more complex than otherwise indicated from bulk measurements and couples to the bad metal nature of this system. It was previously shown using neutron scattering that two magnetic orders coexist below the cluster glasslike transition with the substitution of Sr^{2+} for La^{3+}:[20] a ferromagnetic and commensurate (FMC) one preceding a weak incommensurate (IC) order, yielding a complex phase diagram. In this Brief Report, we examine the relation of magnetic phase separation and transport and the role of the lattice via the ionic size effect.[21] We will show that the development of magnetic superstructures in cobaltites is enhanced with *increasing* $\langle r_A \rangle$ that favors two types of exchange interactions and with consequences on the metallicity.

Nanoscale spin superstructures most readily form in a lattice where local structural disorder brought upon doping large cations makes the FM coupling of spins unstable against AFM order. In contrast to manganites in which superstructures dominate the phase diagram of $La_{1-x}Ca_xMnO_3$ (Ref. 22) but not so of Sr or Ba,[23] in the cobaltite system, complex magnetic states are prevalent in $La_{1-x}A_xCoO_3$ with Ba and Sr but not with Ca. The results of the elastic neutron scattering on single crystals of Ba and Ca show that the development of the IC magnetic state, arising from weak AFM correlations of superexchange interactions between Co^{3+}-Co^{3+} ions concomitantly with the FMC state between Co^{3+}-Co^{4+}, is observed only in Ba and not in Ca crystals. The onset temperatures for the two order parameters initially coincide but as the AFM order grows in strength and becomes commensurate with increasing hole concentration, the FM transition precedes the AFM one. It is also possible and consistent with the results that the charge distribution is confined on FM paths made of DE-coupled Co^{3+}-Co^{4+} ions and could explain the bad metallic nature of this system. On the other hand, in the Ca crystals, the absence of competing interactions leads to larger FM domains.

The single crystals of Ba (x=0.03, 0.06, 0.10, 0.15, and 0.18) and Ca-doped (x=0.05,0.10) cobaltites were grown using a floating-zone image furnace. The crystals varied in size with weights ranging from 5 to 10 g. The neutron mea-

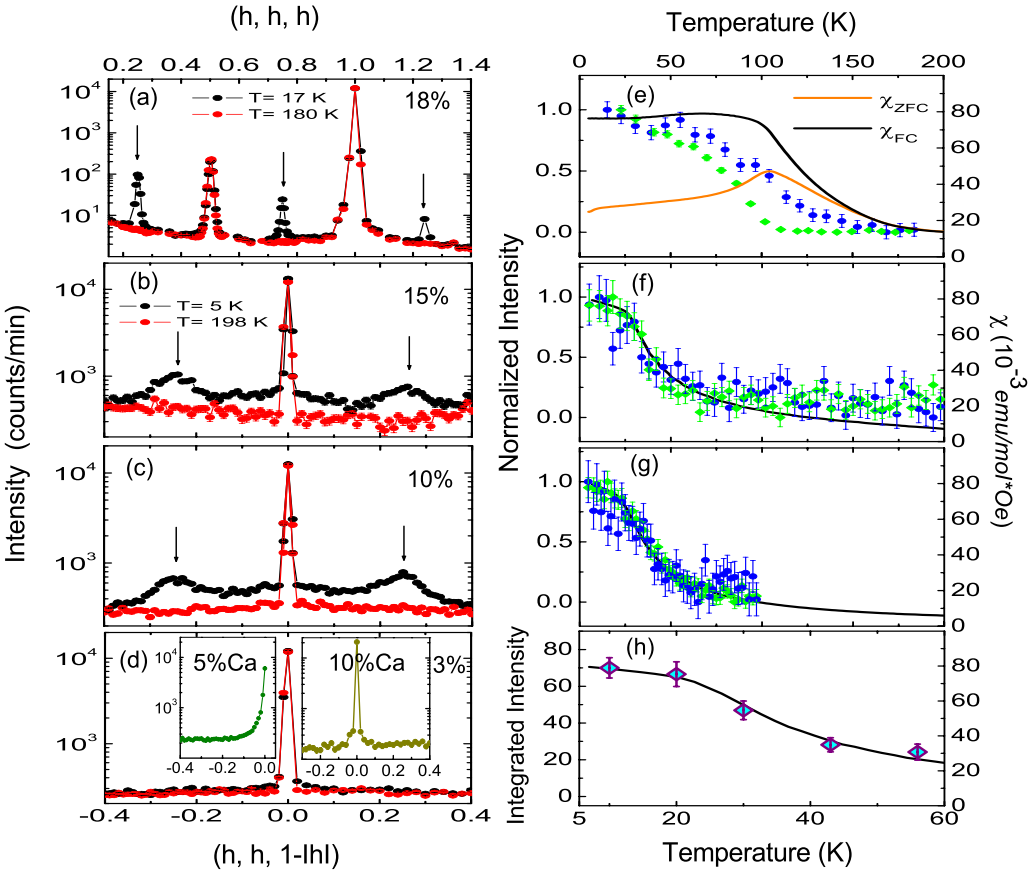

FIG. 1. (Color online) The scans along (h,h,h) shown for (a) $x=0.18$ were collected at TOPAN at the temperatures shown, and along $(h,h,1-|h|)$ for (b) 0.15, (c) 0.10, and (d) 0.03 of the Ba crystals, and 5 and 10% Ca shown in the inset of (d) were collected at SPINS at the temperatures shown in (b). Measurements above T_{SG} are shown in red, while those performed below are shown in black. Broad satellite peaks are present in the low-temperature scans for $x=0.10$ and 0.15 (also for 0.06 but is not shown here) while they become Bragg-like for $x=0.18$. No satellite features are evident in the $x=0.03$ as well as in both of the Ca crystals as seen from the scans at 5 K shown in the inset of (d). The order parameters of the two magnetic signals, the satellite (green), and ferromagnetic (blue) components, are shown in (e) $x=0.18$, (f) 0.15, and (g) 0.10. The order parameter is rescaled to 0:1 by $(I\text{-}I_{\min})/I_{\max}$. These are compared to FC χ_{bulk} at 1000 Oe for the $x=0.10$ and 0.15. In (e), FC and ZFC curves are shown for data collected at 100 Oe. The cusp observed in the ZFC curve coincides with the onset temperature of the satellite peaks. Shown in (h) is the integrated intensity which is proportional to the volume fraction as a function of temperature for the $x=0.10$ and compares well with χ_{bulk}. Error bars represent ± 1 sigma.

surements were carried out using the cold triple-axis spectrometer SPINS at the NIST Center for Neutron Research with a fixed $E_f=3.6$ meV, the thermal spectrometer TOPAN of Tohoku University at the JRR-3 reactor of the Japan Atomic Energy Agency with a fixed $E_f=13.5$ meV, and the HB-1 spectrometer with a fixed $E_f=14.7$ meV at the High Flux Isotope Reactor of the Oak Ridge National Laboratory. The pseudocubic notation is used to analyze the data and the elastic intensity, indicative of static correlations in the time scale of the neutron experiment, was measured in the (hhl) plane. The results summarized in Figs. 1(a)–1(h) reflect the evolving magnetic nature with x as well as provide a contrast of the magnetic state by varying the ionic size at the A site. For data collected above the spin-glass transition temperature, T_{SG}, only the nuclear Bragg peaks are present: in (a), the pattern from TOPAN plotted along (h,h,h) shows the (0.5,0.5,0.5) (which is a $\lambda/2$ reflection) and (111) peaks while in (b)–(d), the cuts along $(h,h,1-|h|)$ from SPINS shows the (001) peak. Below T_{SG} (black symbols), three distinct changes become evident with the increasing hole concentration: first, the Bragg peak integrated intensity increases due to the magnetic contributions. We previously determined that the magnetic scattering is isotropic and originates from static FM correlations.[18] Second, an elastic diffuse scattering intensity is present in crystals with $x=0.06-0.15$ (shown for $x=0.10$ and 0.15) and emanates from the (001) Bragg peak but is either absent or too weak to be detected in the $x=0.18$. Third, satellite peaks of magnetic origin since they follow the Co magnetic form factor are discernible in crystals with $x=0.06$ (not shown), 0.10, 0.15, 0.18 but not in the smallest concentration of 0.03. At the same time, drastic changes in the magnetic structure take place between the 0.15 [Fig. 1(b)] and 0.18 [Fig. 1(a)], namely, the satellite peaks, initially broad, become extremely sharp and Bragg-like, reflecting a transition from short-range to long-range ordering of the second magnetic phase as will be discussed below. The satellite peaks were also observed in a powder sample of $x=0.18$ and cannot be due to chemical clustering.[24] When $\langle r_A \rangle$ is reduced with the substitution of Ca for La, the most distinct change observed by cooling below

T_{SG} is an increase in the magnetic intensity due to static FM correlations. *However*, no satellite peaks are observed in the Ca crystals of $x=0.05$ and 0.10, as can be seen from the two insets of Fig. 1(d) in spite of the fact that different planes in addition to the (*hhl*) were searched. Thus the enhancement of static magnetic superstructures upon nominally increasing $\langle r_A \rangle$ points to intrinsic differences of the 3*d* manifold from the one in manganites.

The FM order parameter is compared to the field-cooled (FC) bulk magnetic susceptibility (solid line), χ_{bulk}, measured using a small piece cut from the same crystals along with the temperature dependence of the normalized intensity at one of the satellite peaks [Figs. 1(e)–1(h)]. All Ba crystals are in the spin-glass phase as is evident from the χ_{bulk} and the system does not become a ferromagnet by 0.18 as in the case of Sr-doped cobaltite.[25] FM intensity is observed in crystals with $x \geq 0.06$ and not below[26] and the onset temperatures for the FM and satellite components overlap while, at the same time, follow the χ_{bulk} [Figs. 1(f) and 1(g)] up to $x=0.15$. Figure 1(h) is a plot of the temperature dependence of the integrated intensity of the $x=0.1$ crystal through the $(\sim 0.25, \sim 0.25, \sim 0.75)$ satellite peak using data collected at HB-1 that clearly shows its one-to-one correspondence to χ_{bulk}. However by $x=0.18$, the FM phase appears first at $\sim$135 K followed by the AFM transition at $\sim$105 K. The FM onset temperature is around the upturn of the field-cooled χ_{bulk} curve while the cusp observed in the zero-field-cooled (ZFC) curve $\sim$105 K coincides with the AFM transition.[27]

The two magnetic signatures coexist in spite of the large compositional changes while the incommensurate modulation wave vector of the superlattice peaks defined as (δ, δ, δ) becomes commensurate. Scattering is observed at four satellite positions, $(h \pm \delta, h \pm \delta, l \pm \delta)$, that order along (111), and δ increases with x as seen in Fig. 2(a). When compared to the x dependence of the incommensurability previously found in Sr-doped crystals, it is clear that δ changes at a much slower rate in Ba crystals and appears to level off at 0.25 r.l.u. In Fig. 2(b), the order parameters for the satellite and FM peaks are plotted as a function of x, where the drastic split of the two is clearly visible at 0.18. The normalized intensity at one of the satellites is compared with that of the (001) Bragg peak as shown in Fig. 2(c) after subtracting the data above the transition that removes the nuclear contribution. Note that the (0.25,0.25,0.25) satellite was used for the 0.18 crystal while the (0.25,0.25,0.75) was used for all other crystals and the normalized intensity was corrected by the square of the magnetic form factor. *Initially*, the IC phase is weaker in comparison to the FMC one. However at $x=0.18$, the satellite peaks become resolution limited and the normalized intensity increases sharply. The correlation length, ξ, of the satellite and FM peaks is estimated from the width of Lorentzian curves fit along the (00L) direction [Fig. 2(d)]. Initially ξ increases slowly with x and is comparable in the two phases, leveling off at $x=0.15$ but rises sharply by 0.18 and becomes quite long for both phases.

The simple ionic picture does not apply well in this system and the DE mechanism fails to couple the FM and metallic behaviors strongly. This can be inferred from the dependence of the correlation length for the two magnetic

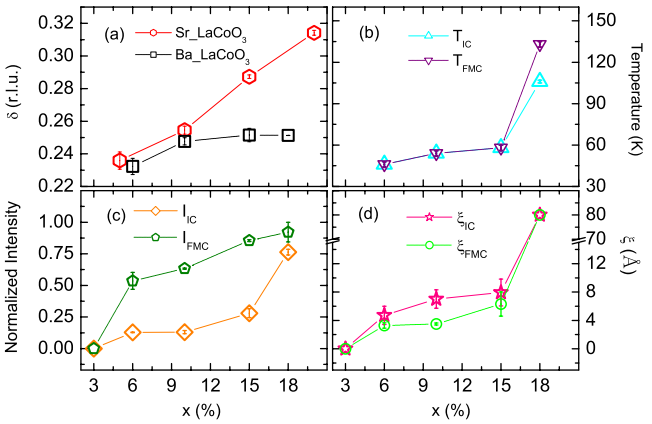

FIG. 2. (Color online) Data for the Ba crystals as a function of hole concentration. (a) is a plot of the IC peak position, δ, with $x\%$ which is compared to the δ dependence on $x\%$ obtained previously for Sr crystals. (b) is a plot of the order parameter for the two magnetic phases. (c) is a plot of the normalized satellite peak intensity, I_{IC} and the (001) Bragg peak, I_{FMC}. The I_{IC} was determined from the integrated peak area of a Lorentzian fit along the (111) direction through the IC peak while the FMC intensity was determined from the integrated peak area of a Lorentzian fit along the (00L) direction through (001). For the normalization by the nuclear Bragg peak, intensity from a longitudinal scan through the Bragg peak and a contribution due to the mosaic of the crystal from the scan along the transverse direction was taken into account. Also, since data were collected at two different energies at TOPAN and SPINS, a $\sin(2\theta)_{magnetic}/\sin(2\theta)_{nuclear}$ term needed to be applied for the satellite peaks to be properly scaled. This was not necessary for the FM peak. (d) is a plot of a comparison of the incommensurate, ξ_{IC} and commensurate, ξ_{FMC}, correlation lengths. Note that ξ is comparable in the two magnetic phases at all x while the value of 80 Å for the 18% is a lower bound since in the experimental setup of TOPAN, the peaks became resolution limited.

signatures and the magnetic moment with $\langle r_A \rangle$ (see Fig. 3). In the absence of a second magnetic transition as with small $\langle r_A \rangle$, the FMC phase has the longest ξ and the largest moment as seen in Fig. 3. This is an unexpected outcome be-

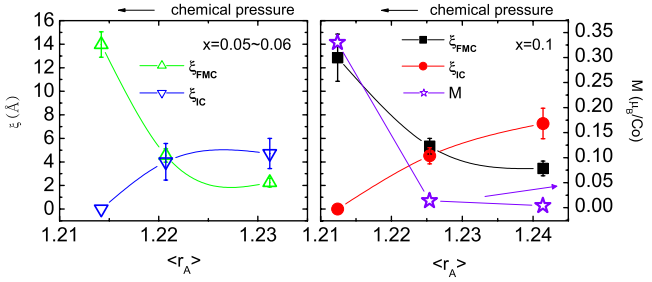

FIG. 3. (Color online) The correlation length, ξ, as a function of $\langle r_A \rangle$, determined for the two magnetic components in Ca, Sr, and Ba crystals of 5(6) and 10%. In determining $\langle r_A \rangle$, the average $\langle A \rangle$ site nine-coordinated radius was used using the appropriate concentration of Co^{3+}/Co^{4+}. At a constant hole concentration, ξ_{FMC} is always larger in Ca than in Sr and Ba crystals. No second magnetic phase has been detected in Ca. At the same time, as $\langle r_A \rangle$ increases, ξ_{FMC} and ξ_{IC} become comparable. The lines are guides to the eye. Also shown on the right panel are values of the magnetization from Ref. 30.

cause chemical pressure as with application of external pressure[28] is expected to increase the crystal field energy, Δ_{CF}, between the t_{2g} and e_g levels favoring a nonmagnetic state. Thus, the negative pressure might induce mixing of the t_{2g} and e_g orbitals that enhances FM coupling due to a stronger Hund intra-atomic exchange, J_{ex}. With increasing $\langle r_A \rangle$, ξ of the FMC phase becomes shorter since it competes with the presence of the second phase and the magnetic moment goes down. To understand these differences, let us first consider the role of the commensurate phase: if a superstructure tries to nucleate in a lattice that has a high tendency for FM order, the incompatibility of the two phases builds up substantial lattice strain that prevents the growth of the superstructure. This can explain why no superstructures appear in Ca crystals where strong FM correlations develop even at low concentrations, much lower than in Sr and Ba crystals.[29] Doping with larger ions such as Sr and Ba however increases the local randomness due to ion size mismatch while the spin-glass phase extends to higher hole concentrations. Because of the randomness of the magnetic phase, AFM magnetic nanoclusters are able to grow into larger entities simultaneously with the FM clusters. The inhomogeneous magnetism observed with increasing $\langle r_A \rangle$ must also be responsible for the bad metallic nature because charge mobility is hindered in the absence of a uniform magnetic structure. How about in Ca crystals then where conductivity is comparable to Sr and Ba crystals?[30] The strong bending of the Co-O-Co bond in the orthorhombic symmetry must reduce electron hopping.[29,30] Inhomogeneous magnetism has been observed in chemically homogeneous systems (without doping) as well as in $Sr_3CuIrO_{6+\delta}$.[31]

Two dramatic features are present in the cobaltites that are important in determining the magnetic state: one is the tendency for AFM domains to grow with $\langle r_A \rangle$ that in turn represents an increase in the local randomness due to the atom size mismatch at the *A* site; and two, the number of FM- and AFM-coupled Co ions increases with the carrier concentration. What can explain the differences among the Ca, Sr, and Ba crystals? The randomness induced by introducing larger ions than La^{3+} at the *A* site gives rise to variable hopping integrals that effectively weakens the FM DE coupling allowing for other interactions to take place. The local randomness is minimal with Ca doping but the increase in the chemical pressure brings upon changes in Δ_{CF} and J_{ex}. In conclusion, the nature of the magnetic state in cobaltites is intricately related to subtle lattice changes. The presence of two magnetic signatures may reflect an electronically phase separated state where the transition from the FM to the IC state involves a redistribution of charge.

The authors would like to thank S. Ishihara, Y. Murakami, and H. Nakao for useful discussions. They thank E. Dagotto for critical reading of the manuscript and H. J. Kang and T. Hong for help with some of the experiments performed at NIST and ORNL. This work is supported by the U. S. Department of Energy under Contract No. DE-FG02-01ER45927, the U.S. DOC through Grant No. NIST-70NANB5H1152, the IMI Program of the National Science Foundation under Grant No. DMR04-09848, and by the Division of Scientific User Facilities, Office of Basic Energy Sciences.

*Corresponding author; louca@virginia.edu

[1] E. Dagotto, Science **309**, 257 (2005).
[2] J. M. Tranquada *et al.*, Nature (London) **375**, 561 (1995).
[3] J. P. Attfield, Nature (London) **396**, 655 (1998).
[4] M. Rini *et al.*, Nature (London) **449**, 72 (2007).
[5] M. Fujita *et al.*, Phys. Rev. B **70**, 104517 (2004).
[6] M. Fujita, H. Goka, M. Enoki, and K. Yamada, Physica B **403**, 1044 (2008).
[7] E. J. Verwey, P. W. Haayman, and F. C. Romeijn, J. Chem. Phys. **15**, 181 (1947).
[8] R. J. McQueeney *et al.*, Phys. Rev. Lett. **100**, 069901(E) (2008).
[9] R. D. Shannon, Acta Crystallogr., Sect. A: Cryst. Phys., Diffr., Theor. Gen. Crystallogr. **32**, 751 (1976).
[10] M. Uehara, S. Mori, C. H. Chen, and S.-W. Cheong, Nature (London) **399**, 560 (1999).
[11] P. Littlewood, Nature (London) **399**, 529 (1999).
[12] H. Kawano *et al.*, Phys. Rev. Lett. **78**, 4253 (1997).
[13] C. P. Adams *et al.*, Phys. Rev. Lett. **85**, 3954 (2000).
[14] T. Egami and D. Louca, J. Supercond. **13**, 247 (2000).
[15] H. Y. Hwang *et al.*, Phys. Rev. Lett. **75**, 914 (1995).
[16] A. J. Millis, Nature (London) **392**, 438 (1998).
[17] P. M. Raccah and J. B. Goodenough, Phys. Rev. **155**, 932 (1967).
[18] D. Phelan *et al.*, Phys. Rev. Lett. **96**, 027201 (2006).
[19] C. Zener, Phys. Rev. **82**, 403 (1951).
[20] D. Phelan *et al.*, Phys. Rev. Lett. **97**, 235501 (2006).
[21] The ionic size effect is a measure of the transfer integral through the bending of the Co-O-Co bond.
[22] P. Schiffer, A. P. Ramirez, W. Bao, and S.-W. Cheong, Phys. Rev. Lett. **75**, 3336 (1995).
[23] C. Martin, A. Maignan, M. Hervieu, and B. Raveau, Phys. Rev. B **60**, 12191 (1999).
[24] P. Tong and Despina Louca (unpublished). Diffraction measurements at BT-1 under field confirmed the presence of the satellite peaks in a powder sample along with their field dependence. Magnetic refinement yields two magnetic cells and not a canted magnetic state.
[25] D. Louca *et al.*, Phys. Rev. B **60**, 10378 (1999); D. Louca and J. L. Sarrao, Phys. Rev. Lett. **91**, 155501 (2003).
[26] For the $x=0.03$ sample, no FM intensity was discernible in the neutron measurement and no spin-glass transition was detected in χ_{bulk} either.
[27] The difference in FC and ZFC curves were previously reported in the Sr-doped system by M. Itoh, I. Natori, S. Kubota, and K. Motoya, J. Phys. Soc. Jpn. **63**, 1486 (1994).
[28] I. Fita *et al.*, Phys. Rev. B **71**, 214404 (2005).
[29] D. Phelan *et al.*, Phys. Rev. B **76**, 104111 (2007).
[30] M. Kriener *et al.*, Phys. Rev. B **69**, 094417 (2004).
[31] A. Niazi, P. L. Paulose, and E. V. Sampathkumaran, Phys. Rev. Lett. **88**, 107202 (2002).